

Revision 2

Error sources in single-clinopyroxene thermobarometry and a mantle geotherm for the Novinka kimberlite, Yakutia

Luca Ziberna^{a,b*}, Paolo Nimis^b, Dmitry Kuzmin^{c,d}, Vladimir G. Malkovets^{c,d}

^a School of Earth Sciences, University of Bristol, Wills Memorial Building, Queen's Road, Bristol BS8 1RJ, United Kingdom

^b Dipartimento di Geoscienze, Università di Padova, Via G. Gradenigo 6, 35131 Padova, Italy

^c V. S. Sobolev Institute of Geology and Mineralogy, Siberian Branch of Russian Academy of Sciences, 3 Koptuyga prospect, Novosibirsk 630090, Russia

^d Novosibirsk State University, 2 Pirogova Str., Novosibirsk 630090, Russia

ABSTRACT

A new suite of 173 clinopyroxene grains from heavy-mineral concentrates of the diamondiferous Novinka kimberlite (Upper Muna field, Yakutia) has been analyzed for major and minor elements with an electron microprobe to perform a thermobarometric study and model the thermal structure of the Proterozoic Upper Muna lithospheric mantle. Scrupulous evaluation of propagation of analytical uncertainties on pressure estimates revealed that (i) the single-clinopyroxene geobarometer can be very sensitive to analytical uncertainties for particular clinopyroxene compositions, and that (ii) most clinopyroxenes from Novinka have compositions that are sensitive to analytical uncertainties, notwithstanding their apparent compositional suitability for single-clinopyroxene thermobarometry based on previously proposed application limits. A test on a variety of mantle clinopyroxenes containing different proportions of the sensitive elements Cr, Na and Al allowed us to identify clinopyroxene compositions that produce unacceptably high propagated errors and to define appropriate analytical conditions (i.e., higher beam currents and longer counting times for specific elements) that allow precise P - T estimates to be obtained for sensitive compositions. Based on the results of our analytical test, and taking into account the intrinsic limitations of the single-clinopyroxene thermobarometer, we have designed a new protocol for optimum thermobarometry, which uses partly revised compositional filters. The new protocol permits precise computation of the

30 conductive paleogeotherm at Novinka with the single-clinopyroxene thermobarometer of Nimis and
31 Taylor (2000). Thermal modeling of the resulting P - T estimates indicates a ~ 34 -mW/m² surface heat
32 flow, a thermal lithosphere thickness of ~ 225 km, and an over 100 km-thick ‘diamond window’
33 beneath Novinka in the middle Paleozoic (344–361 Ma). We estimate that appropriate analytical
34 conditions may extend the applicability of single-clinopyroxene thermobarometry to over 90% of
35 clinopyroxene-bearing garnet peridotites and pyroxenites and to $\sim 70\%$ of chromian-diopside inclusions
36 in diamonds. In all cases, application to clinopyroxenes with $\text{Cr}/(\text{Cr} + \text{Al})_{\text{mol}} < 0.1$ is not recommended.
37 We confirm the tendency of the single-clinopyroxene barometer to progressively underestimate
38 pressure at $P > 4.5$ GPa.

39 **Keywords:** Geobarometry, Chromian diopside, Lithospheric mantle, Palaeogeotherms

40 INTRODUCTION

41 Over the last few decades, thermobarometry of rocks and minerals derived from Earth’s mantle has
42 represented a fundamental tool for the evaluation of the thermal state and structure of sub-craton and
43 off-craton lithospheric sections (e.g., Boyd 1973, 1984; O’Reilly and Griffin 1985; Boyd et al. 1997;
44 Kopylova et al. 1998; Griffin et al. 1999, 2002, 2004; Lazarov et al. 2009; Janney et al. 2010), as well
45 as for the assessment of their diamond potential (e.g., Read et al. 2004; Read and Janse 2009;
46 Cookenboo and Grütter 2010). Deep-seated mantle samples mostly occur as discrete xenoliths or
47 xenocrysts in alkaline magmatic rocks, as isolated grains in sediments derived from their weathering
48 and disruption, and as monomineralic or polymineralic inclusions in kimberlite- and lamproite-borne
49 diamonds. Only the relatively rare discrete xenoliths and polymineralic inclusions in diamonds may be
50 suitable for conventional, two-phase thermobarometry. Single-mineral thermometer–barometer pairs,
51 such as those available for peridotitic garnet and clinopyroxene (Ryan et al. 1996; Nimis and Taylor
52 2000; Grütter et al. 2006), permit thermobarometric surveys to extend across copious data for mantle-
53 derived xenocrysts. Although with some limitations concerning their reliability and applicability (e.g.,

54 Cookenboo and Grütter 2010), the single-mineral methods have enabled the vertical and horizontal
55 mapping of the lithospheric mantle to an extent far beyond that achievable with xenoliths alone (e.g.,
56 Griffin et al. 1999, 2002, 2004; Malkovets et al. 2007; Ashchepkov et al. 2008; Grütter and Tuer 2009;
57 Lehtonen et al. 2009; Nimis et al. 2009; Zozulya et al. 2009).

58 The single-clinopyroxene thermobarometer of Nimis and Taylor (2000) is one of the most used and
59 most reliable single-mineral methods for thermobarometry of disaggregated mantle xenoliths (Nimis
60 2002; Putirka 2008; Grütter 2009; Nimis and Grütter 2010), though its application requires judicious
61 filtering of appropriate clinopyroxene compositions, as well as careful evaluation of the errors
62 associated with calculated temperatures and pressures. Empirically determined compositional filters for
63 single-clinopyroxene thermobarometry were proposed by Nimis and Taylor (2000) and endorsed by
64 Grütter (2009), and low-quality microprobe data were highlighted as responsible for unreliable
65 clinopyroxene thermobarometry outcomes (Grütter 2009; Mather et al. 2011). However, the source of
66 the decreased reliability of single-clinopyroxene thermobarometry for particular compositions has
67 never been investigated in detail. In this contribution, we assess the various sources of error that may
68 affect single-clinopyroxene barometry and propose a new protocol for optimal single-clinopyroxene
69 thermobarometry which specifically considers analytical errors and uses partly revised compositional
70 filters. We then use our results to define a precise conductive geotherm for the diamondiferous Novinka
71 kimberlite, Yakutia, based on high-quality electron microprobe analyses of 97 chromian diopside
72 xenocrysts, selected out of an initial suite of 173 chromian diopside grains. We show that previously
73 proposed compositional filters are sufficient for routine evaluation of mantle geotherms using data for
74 large populations of mantle-derived clinopyroxenes, but that high-quality chemical analyses
75 significantly improve the precision of the individual P - T estimates for fairly common chromian
76 diopside compositions.

77

78 **GEOLOGICAL OUTLINE AND PRELIMINARY SAMPLE SELECTION**

79 The Upper Muna kimberlite field is located at the northern limb of the Markha Terrane, in the central
80 part of the Siberian Craton, and is one of the thirteen fields that form the SW–NE Daldyn–Olenek
81 kimberlite corridor (Fig. 1). This kimberlite field is composed of twenty kimberlite bodies intruded in
82 the Upper Cambrian limestones of the sedimentary cover of the Siberian Platform and is related to the
83 Late Devonian-Early Carboniferous episode of kimberlite magmatism on the Siberian platform (Davis
84 et al. 1980; Agashev et al. 2004; Sun et al. 2014). Recent age determinations gave a narrow interval of
85 kimberlite formation from 361 to 344 Ma (Griffin et al. 1999; Levchenkov et al. 2005; Lepekhina et al.
86 2008a,b; Malkovets VG, unpublished data). For the Novinka kimberlite, SHRIMP analyses of
87 groundmass perovskites gave a U–Pb age of 355 ± 11 Ma (Lepekhina et al. 2008b). One of the striking
88 features of the Upper Muna kimberlite field is that most of the bodies are diamondiferous. All the
89 kimberlite bodies are characterized by abundant fresh deep-seated xenocrysts and xenoliths, but
90 eclogite and crustal xenoliths are very rare.

91 The samples for this study were collected from five sites in the quarry left after bulk sampling
92 inside the contour of the pipe at the present surface and are believed to be a representative mixture of
93 all exposed kimberlite types presently recognized at Novinka. A total of 173 fresh green clinopyroxene
94 grains were picked from the 0.3 to 1.5-mm fraction of heavy-mineral concentrates separated using
95 bromoform at the VS Sobolev Institute of Geology and Mineralogy, Siberian Branch Russian Academy
96 of Sciences, Novosibirsk, Russia. Preliminary major element analyses were performed on these grains
97 using a JEOL Superprobe JXA-8200 electron microprobe (hereafter, EMP) housed at the Max Planck
98 Institute for Chemistry, Mainz, Germany. Operating conditions and compositions for all 173 grains are
99 reported in the Supplementary Table S1.

100 **OPTIMIZED PROTOCOL FOR PRECISE SINGLE-CLINOPYROXENE THERMOBAROMETRY**

101 **Source of errors and compositional filters**

102 The single-clinopyroxene thermobarometer uses a combination of the enstatite-in-Cpx thermometer
103 and Cr-in-Cpx barometer (Nimis and Taylor 2000). The enstatite-in-Cpx thermometer has proved a
104 top-quality method when compared to other mantle geothermometers (Nimis and Grütter 2010) and has
105 limited sensitivity to analytical uncertainties (Nimis 2002). The Cr-in-Cpx barometer suffers from two
106 major drawbacks: i) evaluations against experiments have shown progressive underestimation of the
107 equilibrium pressures above ca. 4.5 GPa (up to 0.6–1.0 GPa at 7.0 GPa; Nimis 2002); ii) deviations
108 from results of orthopyroxene–garnet barometry on the same xenolith samples can be very large for
109 clinopyroxenes characterized by low values of $a_{Cr} = Cr - 0.81 \cdot (Na + K) \cdot Cr / (Cr + Al)$ atoms per 6-
110 oxygen formula unit (hereafter apfu), which is the main building block in the barometer formulation
111 (Fig. 2). Low a_{Cr} values at high P/T ratios in the calibration database, a molar volume change for the
112 reaction involving garnet and clinopyroxene (cf. equation 1 in Nimis and Taylor 2000) less than one-
113 half that of common orthopyroxene-based barometers (cf. Brey et al. 1990), and the intrinsic
114 limitations of being an empirical single-mineral method account for the lower precision of the Cr-in-
115 Cpx barometer (cf. Figs. 1c,d in Grütter 2009). More generally, these drawbacks may explain why $P-T$
116 estimates using the single-clinopyroxene methods are often more scattered compared to those using
117 conventional thermobarometers (cf. Stachel and Harris 2008; Eaton et al. 2009; Shirey et al. 2013).

118 Apart from the above issues, safe application of the single-clinopyroxene method requires a careful
119 selection of the samples, in order to exclude compositions outside the range used for the calibration or
120 too sensitive to analytical uncertainties. Grütter (2009) compiled and partly modified compositional
121 and related filters designed by various authors that serve as a useful ‘cookbook’ to eliminate
122 unwarranted data from consideration for $P-T$ calculations. The filters include: (i) total cations per 6
123 oxygens in the range 3.96–4.04, slightly more permissive than the 3.98–4.02 range advised by Nimis
124 and Taylor (2000); (ii) Cr_2O_3 vs Al_2O_3 relationships within the garnet-peridotite field of Ramsay and
125 Tompkins (1994); (iii) Al_2O_3 vs MgO relationships within the high-Al field of Nimis (1998); (iv) $Cr\#$
126 in the range 0.06–0.50; (v) $a_{Cr} \geq 0.003$ apfu. Filter (i) serves to exclude obviously poor-quality

127 analyses, which may result from poor EMP standardization, bad sample preparation, contamination
128 from inclusions, etc. In this work we revert to the more restrictive 3.98–4.02 cation range to promote
129 high-quality P – T estimates for individual clinopyroxene grains. Filters (ii) and (iii) serve to exclude
130 clinopyroxenes that may not have been in equilibrium with garnet. Filters (iv) and (v) exclude
131 compositions falling well outside the range of the experiments used for the calibration of the Cr-in-Cpx
132 barometer, which included clinopyroxenes with $Cr\# = 0.09$ – 0.44 , and $a_{Cr} = 0.003$ – 0.087 apfu (Nimis
133 and Taylor 2000). As originally suggested by Nimis and Taylor (2000), the removal of clinopyroxenes
134 with $a_{Cr} < 0.003$ apfu should also help to exclude compositions that are too sensitive to propagation of
135 analytical errors. We will show that filters (iv) and (v) require revision.

136 Figure 2 shows that the threshold $a_{Cr} \geq 0.003$ apfu suggested by Nimis and Taylor (2000) and
137 adopted by Grütter (2009) may be too optimistic: at $a_{Cr} = 0.010$ apfu, deviations from the
138 orthopyroxene–garnet pressures calculated for the same well-equilibrated mantle xenoliths may be as
139 high as ± 1.0 GPa, reaching ± 3.0 GPa for $a_{Cr} < 0.003$ apfu. This shortcoming is particularly relevant for
140 the study of Novinka chromian diopsides. Based on preliminary microprobe analyses of 173 grains
141 (Supplementary Table S1), 118 grains satisfy the compositional criteria for derivation from garnet
142 peridotite [i.e., filters (ii) and (iii)], with 39 of 118 (33%) having $a_{Cr} \leq 0.003$ apfu, and 107 of 118
143 (91%) having $a_{Cr} \leq 0.010$ apfu. Observing the latter threshold would therefore render most of our
144 Novinka samples unsafe for thermobarometry. In principle, the decreased precision of the Cr-in-Cpx
145 barometer at low a_{Cr} may be due to an oversimplified treatment of Cr equilibria between clinopyroxene
146 and garnet or it may reflect an excessive sensitivity of the method to analytical errors or to departures
147 from chemical equilibrium. Mather et al. (2011) made a semi-quantitative evaluation of the influence of
148 analytical errors, but they did not account for their dependence on absolute element concentrations and
149 analytical conditions (cf. Potts 1983 and Appendix of this work). In the present work, we have made an
150 analytical test to quantitatively assess the propagation of analytical errors on pressure estimates (see
151 Appendix for details): multiple EMP analyses on compositionally diverse clinopyroxenes using

152 different analytical conditions demonstrated that (i) the decreased precision of the Cr-in-Cpx barometer
153 for clinopyroxenes with low a_{Cr} values is largely related to propagation of analytical errors, (ii) the
154 analytical errors, as expected, increase smoothly with decreasing beam current and counting times, and
155 (iii) the propagated P uncertainties are negatively correlated with the clinopyroxene a_{Cr} parameter and
156 positively correlated with the clinopyroxene Cr/(Cr + Al) molar ratio ($Cr\#$) (Fig. 3). Therefore, the
157 $a_{Cr}/Cr\#$ parameter, rather than the previously used a_{Cr} parameter, is a more reliable indicator of the
158 sensitivity of single-clinopyroxene barometry to analytical uncertainties. Minimum conditions for
159 electron microprobe analysis were thus defined for different values of the $a_{Cr}/Cr\#$ parameter (Table
160 A2), which maintain propagation of analytical uncertainties within acceptable limits (defined here as \pm
161 0.25 GPa).

162 A further assessment of the importance of analytical errors on Cr-in-Cpx P estimates can be made
163 using mantle xenoliths as test cases. Based on the results of our analytical tests (see Appendix), we
164 have refined the database of well-equilibrated xenoliths of Nimis and Grütter (2010) by excluding those
165 clinopyroxene analyses for which the estimated P uncertainties were unsatisfactorily high. For each
166 record, the analytical errors on Al, Cr, and Na concentrations in the clinopyroxene were calculated
167 taking into account the analytical conditions used for the analysis as reported in the source papers, and
168 the corresponding P uncertainties were calculated through error propagation. If the reported analytical
169 conditions did not match exactly any of those utilized here, the errors were estimated by interpolation
170 of values obtained by assuming lower and higher beam currents or counting times. For records for
171 which analytical details had not been reported, we cautiously assumed the beam current and counting
172 times to be the lowest (i.e., 15 nA, 10 s peak, 10 s background). The records for which the model P
173 uncertainties were greater than \pm 0.25 GPa were discarded. Clearly, the model P uncertainties may not
174 be strictly accurate, since different analytical equipments were used for the analyses. However, the
175 above screening certainly excluded most of the records for which single-clinopyroxene P - T estimates
176 are probably unreliable. Figure 4 shows that the discrepancies between Cr-in-Cpx and orthopyroxene-

177 garnet pressures are greatly reduced for the refined database, especially at pressures above 3 GPa, thus
178 supporting the major role of propagation of analytical errors on P uncertainties. At lower pressures,
179 significant deviations are still observed only for a few samples with $Cr\# < 0.1$ (Fig. 4b), which suggests
180 poor reliability of the Cr-in-Cpx barometer for these low- $Cr\#$ compositions. This may be related to the
181 fact that the Cr-in-Cpx barometer was calibrated on 120 experimental clinopyroxenes with $Cr\#$ in the
182 range 0.09–0.44, with only 6 of them having $Cr\# < 0.1$ (Nimis and Taylor 2000). The original
183 minimum threshold of 0.06 for $Cr\#$ suggested by Grütter (2009) thus appears to be too permissive.
184 Examination of Figure 4b also reveals that clinopyroxenes with $Cr\#$ as high as 0.65 do not show any
185 systematic deviation from orthopyroxene–garnet P . This suggests that the upper limit for $Cr\#$ of 0.50
186 proposed by Grütter (2009) is excessively restrictive, despite the fact that the Cr-in-Cpx barometer was
187 calibrated on clinopyroxenes with $Cr\# \leq 0.44$.

188 An additional problem when investigating loose mineral grains is to assess whether the
189 clinopyroxene was in equilibrium with orthopyroxene, a condition necessary for single-clinopyroxene
190 thermometry. Recognition of orthopyroxene-saturated samples is not straightforward and was not
191 explicitly addressed by Grütter (2009). Based on the above considerations, we propose a partly revised
192 protocol for sample selection, which takes into account both the intrinsic limitations of the single-
193 clinopyroxene thermobarometers and the uncertainties related to propagation of analytical errors.

194 (1) *General quality test of EMP analysis*: total cations per 6 oxygens in the range 3.98–4.02. Less
195 restrictive limits, such as those suggested by Grütter (2009), might be adopted in some cases, but a
196 possible increase of scatter around geotherms should be considered.

197 (2) *General equilibrium test*: grains exhibiting significant zoning, suggesting disequilibrium,
198 should generally be discarded.

199 (3) *Verification of equilibrium with garnet*: Cr_2O_3 vs Al_2O_3 relationships within the garnet-
200 peridotite field of Ramsay and Tompkins (1994), i.e., $Cr_2O_3 > 0.5$ wt% and $Al_2O_3 \leq 4.0$ wt% (if Cr_2O_3

201 < 2.25 wt%) or ≤ 5.0 wt% (if $\text{Cr}_2\text{O}_3 > 2.25$ wt%). This restriction may produce false negatives. The
202 reliability of single-clinopyroxene methods for anomalously Cr_2O_3 -rich compositions ($\text{Cr}_2\text{O}_3 > 5.0$
203 wt%) is unknown and therefore these compositions should be used with caution.

204 (4) *Further refinement of (3)*: Al_2O_3 vs MgO relationships within the high-Al field of Nimis
205 (1998), i.e., $\text{Al}_2\text{O}_3 \geq 0.7$ wt% and $\text{Al}_2\text{O}_3 \geq 12.175 - 0.6375 * \text{MgO}$ wt% (this parametrization is taken
206 directly from Fig. 3 in Nimis 1998; the slightly different formula suggested by Grütter 2009 provides
207 almost identical results). False negatives may be produced also in this case, especially among diamond-
208 facies samples (cf. Fig. 3 in Nimis 1998).

209 (5) *Rejection of compositions with 'unsafe' Cr# values*: Cr# in the range 0.10–0.65 (replacing the
210 range 0.06–0.50 of Grütter 2009); Cr# values in the range 0.50–0.65 should still be used with caution
211 because of limited testing in this compositional range.

212 (6) *Recognition of compositions sensitive to analytical uncertainties*: $a_{\text{Cr}}/\text{Cr\#} > x$, where x is a
213 function of EMP analytical conditions. Table A2 provides a general guideline for determining x ,
214 although its value may be varied for different analytical equipments based on personal experience. This
215 filter replaces the filter $a_{\text{Cr}} \geq 0.003$ apfu of Nimis and Taylor (2000) and Grütter (2009). If $a_{\text{Cr}}/\text{Cr\#} \leq$
216 0.011 apfu, the clinopyroxenes should generally be discarded; if $0.011 < a_{\text{Cr}}/\text{Cr\#} \leq 0.024$ apfu, high-
217 quality analyses are recommended; if $a_{\text{Cr}}/\text{Cr\#} > 0.024$, propagation of analytical errors is predictably
218 small and therefore routine analyses can safely be used. The range for $a_{\text{Cr}}/\text{Cr\#}$ in the experiments used
219 to calibrate the Cr-in-Cpx barometer of Nimis and Taylor (2000) was 0.016–0.393, therefore excluding
220 compositions with $a_{\text{Cr}}/\text{Cr\#} \leq 0.011$ apfu will also avoid large extrapolations outside the calibration
221 range.

222 (7) *Verification of equilibrium with orthopyroxene*. This cannot be obtained through simple
223 compositional filters. In general, $\text{Ca}/(\text{Ca} + \text{Mg})_{\text{mol}}$ ratios > 0.5 should be considered as suspicious, as a
224 very small proportion of orthopyroxene-saturated chromian diopsides (ca. 1%) lie above this value. A

225 very low estimated T (e.g., <600 °C) would also be a strong indication that the diopside was not in
226 equilibrium with orthopyroxene, which implies underestimation of T using the enstatite-in-Cpx
227 thermometer and, consequently, underestimation of the Cr-in-Cpx P . Following Nimis and Grütter
228 (2010), a cut-off at $T > 700$ °C provides a safer selection of clinopyroxenes for which enstatite-in-Cpx
229 temperatures should be sufficiently reliable.

230 (8) *Identification of potential outliers.* As recommended by Grütter (2009), final examination of P -
231 T plots for a given locality may help to distinguish outliers departing off the general trend, which may
232 conveniently be excluded for the determination of mantle geotherms.

233

234 **Application to Novinka clinopyroxenes**

235 For the purposes of this study, we used the preliminary analyses of Novinka clinopyroxenes (Jeol
236 Superprobe, Mainz; Supplementary Table S1) only for a first compositional screening aimed to
237 eliminate obviously unsuitable analyses. We excluded 55 clinopyroxenes plotting outside the ‘garnet
238 peridotite’ field of Ramsay and Tompkins (1994), which may not be equilibrated with garnet, and 5
239 clinopyroxenes showing very low enstatite contents [$\text{Ca}/(\text{Ca} + \text{Mg})_{\text{mol}} > 0.5$], which are unlikely to be
240 equilibrated with orthopyroxene. In addition, 16 grains that contained abundant melt inclusions, which
241 likely indicate severe interaction with the host kimberlite magma, were also discarded.

242 The remaining 97 grains were re-analysed using a CAMECA SX-50 electron microprobe (EMP;
243 IGG-CNR, Padua, Italy) (see Appendix for details). Compositional data were first collected using a
244 *routine* analytical procedure, which employed an accelerating voltage of 20 kV, a beam current of 15
245 nA, and counting times of 10 s for peak and 10 s for background (i.e., 5 s on each side of the peak), for
246 all elements. Further filtering based on the newly revised protocol was then applied to the results of the
247 routine analyses. We discarded 5 grains showing significant zoning, 9 grains plotting outside the high-
248 Al field of Nimis (1998) and 9 grains showing $a_{\text{Cr}}/\text{Cr}\# < 0.011$. We then re-analyzed 56 clinopyroxenes
249 with $0.011 < a_{\text{Cr}}/\text{Cr}\# \leq 0.024$ using higher beam current (40 nA) and counting times (40 sec for both

250 peak and background) for Al, Cr and Na, and routine EMP conditions for the other elements. Pressures
251 and temperatures were calculated with the thermobarometers of Nimis and Taylor (2000) using the
252 averages of five point analyses. The major element compositions of the peridotitic clinopyroxenes
253 determined using both the routine and the optimized analytical conditions and the relative P - T
254 estimates are reported in the Supplementary Table S2.

255

256

RESULTS

257 Based on the preliminary analyses of the 173 clinopyroxenes (Supplementary Table S1), the majority
258 of the grains (68%) fall into the low-Al, ‘garnet peridotite’ field of Ramsay and Tompkins (1994).
259 About one fourth of these, however, show relationships between Al_2O_3 and MgO contents that are
260 compatible also with an origin from garnet-free, metasomatised lherzolites (cf. Nimis 1998). Another
261 4% fraction of the ‘garnet peridotite’ grains shows high CaO contents (>22 wt.%), high $\text{Ca}/(\text{Ca} +$
262 $\text{Mg})_{\text{mol}}$ ratios (>0.5) and excessively low estimated T (<500 °C) and can be classified as ‘wehrlitic’. A
263 relatively large number of the studied grains (29%) have Cr_2O_3 contents lower than 0.5 wt.%, which
264 would classify them as either ‘eclogitic’ or ‘megacrystic’ (Ramsay and Tompkins 1994). The Na_2O
265 content in these low-Cr grains is generally low to very low (mostly <2.5 wt.%), which is more
266 consistent with a megacrystic/pyroxenitic origin. A very small number of grains (2%) have relatively
267 high Al_2O_3 contents (4.6–5.4 wt.%) and fall in the spinel peridotite field of Ramsay and Tompkins
268 (1994).

269 Grey symbols in Figure 5a show the results of the thermobarometric study of the 97 selected
270 clinopyroxenes using the routine analyses obtained with the CAMECA SX50 (Padua). As expected
271 from the low a_{Cr} values of most clinopyroxenes, the P - T estimates obtained using routine analyses
272 show considerable scatter, especially at $P > 5.0$ GPa (Fig. 5a). Depending on the preferred model
273 geotherm shape, minor to very large thermal perturbations (up to several hundred degrees) may be
274 inferred near the base of the lithosphere. Adopting the revised filtering protocol proposed in this work

275 and using 56 high-quality analyses for clinopyroxenes with $0.011 < a_{Cr}/Cr\# \leq 0.024$, the P - T scatter is
276 considerably reduced (black symbols in Fig. 5a). Ten samples with $Cr\# > 0.50$ and as high as 0.63 do
277 not show any deviation from the overall trend, which supports the reliability of single clinopyroxene
278 thermobarometry for these compositions (cf. also Fig. 4). The refined thermobarometric estimates ($N =$
279 74) span the P - T range 2.3–6.5 GPa and 660–1390 °C, with the majority of the clinopyroxenes falling
280 in the diamond stability field (Fig. 5a). Trimming the data at $T > 700$ °C does not produce any
281 reduction in the overall scatter. A gap is observed in the pressure range 3.3–3.9 GPa, which could be
282 related to a sampling bias of the kimberlite or to absence of clinopyroxene-saturated assemblages in the
283 mantle in this pressure interval.

284 For the sake of comparison, Figure 5b shows the results of the thermobarometric study of the same
285 97 clinopyroxenes, but adopting Grütter's (2009) original filters for $Cr\#$ ($0.06 < Cr\# < 0.5$) and a_{Cr} (\geq
286 0.003 apfu) and using routine analyses for all samples. The results show a marginal increase of scatter
287 and an overall shift of the high- P samples (> 4.0 GPa) to slightly higher P , the average difference being
288 ca. 0.2 GPa. However, differences in P - T estimates for individual grains (routine vs. high-quality
289 analyses) are as high as +0.5 GPa and +50 °C and the total number of 'accepted' clinopyroxenes is
290 reduced to 67.

291

292 THERMAL STATE AND THICKNESS OF THE UPPER MUNA LITHOSPHERIC MANTLE

293 Much of what is known about the thermal state of the mantle beneath the Siberian craton comes from
294 studies of xenoliths from the Daldyn field (Fig. 1), and in particular from the Udachnaya kimberlite.
295 Conventional thermobarometry of mantle xenoliths from this kimberlite indicates low geothermal
296 gradients, corresponding to a surface heat flow of 35–40 mW/m² based on the conductive model of
297 Pollack and Chapman (1977) (hereafter PC77), and deep lithospheric mantle roots (~ 220 km) (Griffin
298 et al. 1996; Boyd et al. 1997; Pokhilenko et al. 1999; Ionov et al. 2010; Goncharov et al. 2012;
299 Agashev et al. 2013; Doucet et al. 2013). Variations in available estimates of the (conductive) mantle

300 geotherm depend in part on the different combinations of thermobarometers used by the different
301 authors and in part on a significant scatter in the reported P – T estimates.

302 Additional slices of information on the Daldyn field and on the nearby Alakit and Upper Muna
303 fields (Fig. 1) were provided by Griffin et al. (1999), who applied the Ni-in-garnet thermometer and
304 Cr-in-garnet barometer (Ryan et al. 1996) to large suites of garnet xenocrysts. Their results suggest a
305 cool geotherm (35 mW/m^2) and a chemical lithosphere thickness of $\sim 240 \text{ km}$ for the Alakit mantle
306 section, similar to that in the Daldyn mantle section, but a slightly higher geotherm (38 mW/m^2) and a
307 thinner lithosphere ($\sim 210 \text{ km}$) for the more northeasterly Upper Muna mantle section. The main
308 limitation of the garnet-based method is that reliable pressure estimates can only be retrieved for Cr-
309 saturated garnets (i.e., garnets in equilibrium with chromite). If this condition is not satisfied, only
310 minimum pressures can be estimated. Therefore, a geotherm is typically obtained by interpolating
311 maximum P estimates determined for each T recorded by a large number of grains. Scatter of
312 individual P – T points and intrinsic uncertainties in the empirical thermobarometer calibrations (Ryan et
313 al. 1996; Canil 1999), however, may limit the accuracy of the interpolation. Moreover, since Cr-
314 saturated garnets are relatively rare in kimberlites and their vertical distribution is not uniform (Griffin
315 et al. 2002; Malkovets et al. 2007), localized thermal perturbations are not easily recognized. More
316 recent P – T estimates for the Upper Muna field were provided by Ashchepkov et al. (2010), using
317 combinations of different thermobarometers. The results were ambiguous, because of the very large
318 scatter of P – T estimates and evident inconsistencies among the different thermobarometers used (see
319 Figs. 18 to 20 in Ashchepkov et al. 2010).

320 Our P – T data for clinopyroxenes provide independent constraints on the thermal state of the Upper
321 Muna lithospheric mantle at the time of eruption of the Novinka kimberlite. Figure 5 shows that the
322 low- T ($< 1100 \text{ }^\circ\text{C}$) clinopyroxenes align along the 40-mW/m^2 model conductive geotherm of PC77,
323 which is slightly warmer than the ‘garnet geotherm’ defined by Griffin et al. (1999) for the Upper
324 Muna field (38 mW/m^2). This is consistent with the observations of Grütter et al. (2006), who

325 demonstrated that the Ni-in-garnet method of Ryan et al. (1996) adopted by Griffin et al. (1999) tends
326 to underestimate mantle geotherms by ~ 2 mW/m². An apparent inflection of the geotherm is observed
327 at $T > 1100$ °C and $P > 5.5$ GPa, with P - T data plotting on or slightly above the 44-mW/m² model
328 conductive geotherm (Fig. 5a). This apparent inflection may partly be an artifact caused by the known
329 P underestimation at high pressures of the Cr-in-Cpx geobarometer (cf. Nimis 2002; see also next
330 Section). More importantly, the still widely used PC77 reference model predicts a stronger curvature of
331 geotherms compared with recent thermal models (cf. Hasterok and Chapman 2011; Mather et al. 2011),
332 and could suggest deviation from a conductive thermal gradient even in unperturbed mantle sections.

333 To derive a robust geotherm for the Upper Muna field, we have fitted the clinopyroxene P - T data
334 using the FITPLOT program (McKenzie and Bickle 1988; McKenzie et al. 2005), as upgraded by and
335 described in Mather et al. (2011). Different from the PC77 reference geotherms, this program allows
336 computing the change in temperature with depth within the thermal boundary layer, allows varying the
337 crustal thickness and heat production in the crust and mantle, and includes updated models for the
338 temperature dependence of thermal conductivity. Moreover, the surface heat flow is an output of the
339 fitting procedure and not a fixed input value that is used to generate a geotherm. We assumed a crustal
340 thickness of 56 km based on Manakov's (2002) seismic model for the Siberian craton. The mean heat
341 production in the crust was assumed to be 0.36 μ W/m³, in agreement with data reported in Rosen et al.
342 (2009) for the Anabar shield. The heat production rate in the upper mantle was imposed at 0.0 μ W/m³
343 and the potential T for the asthenospheric isentrope was set at 1315 °C, following Mather et al. (2011).
344 The thermal conductivity was assumed to be 2.5 W/m·K throughout the crust. In the mantle, we used
345 the thermal conductivity for olivine at (P , T) of Osako et al. (2004).

346 Comparison of the clinopyroxene P - T data with the calculated geotherm (Fig. 6a) shows an
347 excellent agreement in the intermediate P - T region, with a residual 'inflection' at high P - T . The
348 magnitude of this inflection is compatible with the above-mentioned underestimation of the Cr-in-Cpx
349 barometer at high P (Nimis 2002; see also next Section). Therefore, we interpret the smooth high- P - T

350 inflection as an artifact. To minimize the potential bias due to P underestimation at high P and derive a
351 more refined geotherm, we have re-fitted the P – T data by excluding data plotting above 5.5 GPa.
352 Trimming the data did not produce significant changes in the model geotherm, excepting for an
353 obvious significant reduction of the xenolith misfit and a very slight increase in the calculated
354 lithospheric thickness, as defined by the intersection of the conductive geotherm with the mantle
355 isentrope (Fig. 6b). The agreement between the trimmed P – T data and the model is excellent. The
356 resulting surface heat flow is 34 mW/m² and the base of the thermal lithosphere is at 225 km,
357 corresponding to a T of 1436 °C. The base of the Mechanical Boundary Layer (McKenzie and Bickle
358 1988) is at 204 km depth, corresponding to a T of 1355 °C. Hasterok and Chapman's (2011) geotherm
359 model, which uses a more generalized heat production model for the continental lithosphere, would
360 also provide a good fit to the P – T data and would only suggest a slightly higher surface heat flux of 37
361 mW/m². The computed heat flow is slightly lower than that estimated by simple visual comparison
362 with the PC77 model geotherms (Fig. 6), but it is still significantly higher than the present-day value of
363 ~27 mW/m² (Duchkov and Sokolova 1997). Adopting different cut-off thresholds at high and low P – T
364 did not result in significant modification of the calculated geotherm. The combination of lithosphere
365 thickness and geothermal gradient indicates a large 'diamond window' beneath Novinka, extending
366 from ca. 110 to over 200 km depth in the middle Paleozoic (344–361 Ma).

367 Comparison with thermobarometric data for the nearby, broadly coeval (342–360 Ma; Davis et al.
368 1980) Daldyn kimberlite field (Figs. 6c–e) is hampered by the recognized temperature gap between ca.
369 900 and 1200 °C in P – T estimates for xenoliths from Udachnaya (Doucet et al. 2013), which reduces
370 the robustness of geotherm fitting, and by non-optimized analytical procedures in the literature data.
371 Additional ambiguity derives from minor inconsistencies between estimates obtained using different
372 thermobarometer pairs (cf. Doucet et al. 2013). If the same single-clinopyroxene thermobarometers are
373 used for both data sets, the P – T data for Udachnaya appear to be broadly consistent with the Upper
374 Muna calculated geotherm, although somewhat more scattered at high T (Fig. 6e).

375

376 **GENERAL IMPLICATIONS ON XENOLITH THERMOBAROMETRY AND GEOTHERM EVALUATION**

377 We have shown that careful compositional screening and high-quality analysis of peridotitic
378 clinopyroxenes from the Novinka kimberlite (Upper Muna field, Yakutia) have allowed to reduce
379 thermobarometric uncertainties and to make a good assessment of the thermal state of the lithospheric
380 mantle at the time of kimberlite eruption. It is worth noting, however, that EMP analytical conditions
381 employed in studies of garnet peridotites or diamond inclusions are often not optimized for reliable
382 thermobarometry. Moreover, in many cases, the analytical conditions are not reported or only partial
383 documentation is given. Of twenty-two published papers in which the Cr-in-Cpx barometer is applied
384 and documentation of EMP analytical conditions is provided, twenty used relatively low beam currents
385 (≤ 20 nA) and/or low counting times (≤ 20 s for peak) (e.g., Wang and Gasparik 2001; Menzies et al.
386 2004; Donnelly et al. 2007; Faryad et al. 2009; Nimis et al. 2009; Doucet et al. 2013; Chen et al. 2014).
387 This casts doubts on the reliability of many existing single-clinopyroxene thermobarometric data and
388 demands proper evaluation of propagation of analytical errors on P estimates.

389 Although analytical uncertainties will obviously depend not only on the adopted analytical
390 conditions but also on the performance of the equipment and quality of the standardization routines,
391 simplified thresholds based on compositional parameters reported in Table A2 can be used in common
392 practice to define the most appropriate analytical conditions for thermobarometric applications or to
393 help select the most reliable analyses from published datasets. If low beam current and short counting
394 times are used (e.g., 15 nA, 10 s peak, 10 s background), the safety threshold of $a_{Cr}/Cr\# > 0.024$ apfu
395 would cut off 19% of the 764 records in the mantle xenolith database of Nimis and Grütter (2010) and
396 46% of reported clinopyroxene inclusions in peridotitic and websteritic diamonds (cf. Stachel and
397 Harris 2008). Using higher beam current and longer counting times (e.g., 40 nA, 40 s peak, 40 s
398 background) the threshold may decrease to 0.011 apfu, thus cutting off only 4% of the xenoliths and
399 15% of the inclusions. The $Cr\#$ threshold of 0.1 proposed here cuts off further 5% of the xenoliths

16

400 (mostly pyroxenites) and 17% of the inclusions (almost all from websteritic diamonds). Note that the
401 $a_{Cr}/Cr\#$ ratio decreases with increasing P/T ratio (Fig. 7). Therefore, clinopyroxenes with compositions
402 that are the most sensitive to propagation of analytical errors on estimated P (i.e., those with the lowest
403 $a_{Cr}/Cr\#$) are those equilibrated under conditions corresponding to the highest P/T ratios. This indicates
404 that clinopyroxene geotherms will tend to be less precise for cold cratonic mantle sections if EMP
405 analyses are not of sufficient quality.

406 The effect of poor-quality analyses will tend to average out when a large population of chromian
407 diopsides from a certain locality is used. Therefore, definition of mantle thermal state and diamond
408 potential using the sample selection and analytical strategies proposed here may show only marginal
409 improvement with respect to previously proposed protocols (cf. Grütter 2009). Nonetheless, the
410 proportion of ‘accepted’ samples can be increased, the precision of individual $P-T$ estimates can be
411 improved, and ‘unsafe’ compositions are more effectively recognized (Fig. 5). This represents an
412 advantage when the available population of clinopyroxene data is restricted for some reason (e.g.
413 inclusions in diamonds), or when a detailed comparison between individual $P-T$ estimates is required.

414 It should be emphasized that high-quality analyses *and* appropriate compositional screening will
415 considerably reduce scatter of $P-T$ estimates, but they will not eliminate systematic deviations of Cr-in-
416 Cpx pressures due to inconsistencies in its calibration. In fact, the progressive negative deviation of Cr-
417 in-Cpx P estimates relative to orthopyroxene–garnet P estimates at $P > 4.5$ GPa (Fig. 4) confirms the
418 tendency of the Cr-in-Cpx barometer to underestimate at high P (by ca. 1 GPa at 7 GPa), which was
419 previously observed against a limited set of experimental data (cf. Nimis 2002). Moreover, a slight
420 positive deviation of the Cr-in-Cpx pressures (<0.5 GPa on average) is observed at P around 3 GPa
421 (Fig. 4), which partly confirms observations by Grütter and Moore (2003) and Grütter (2009). It is
422 unclear if this small discrepancy at moderate P is due to inaccuracy of the Cr-in-Cpx barometer, of the
423 orthopyroxene–garnet barometer, or of both. Owing to these systematic deviations, mantle
424 palaeogeotherms calculated on the basis of single-Cpx thermobarometry will tend to show slightly

425 different shapes than those based on orthopyroxene–garnet barometry. The most important
426 discrepancies will affect the deepest portion of the lithosphere, where clinopyroxene geotherms will
427 tend to show slightly overestimated T/P gradients. As discussed by Nimis (2002), this drawback will
428 not hamper recognition of samples coming from the diamond window.

429

430

Acknowledgments

431 The present work is part of LZ's PhD research program at the University of Padova (Italy). The authors
432 are indebted to G. Pearson, L. Franz and to late J. Boyd for supplying materials for the present study,
433 and to R. Carampin (IGG-CNR, Padova) for his invaluable help during analytical sessions. H. Grütter
434 and T. Stachel are thanked for sharing their compilations of xenolith and diamond inclusion data. S.
435 Klemme is thanked for precious suggestions. Formal reviews by H. Grütter and an anonymous referee
436 pointed out some important flaws in our original manuscript and helped us significantly improve this
437 paper. PN acknowledges support by ERC Starting Grant 307322 (project INDIMEDEA). LZ
438 acknowledges support by Fondazione Cassa di Risparmio di Padova e Rovigo – “Progetto Dottorati di
439 Ricerca 2009”. We thank A.V. Sobolev for the given opportunity to perform analytical procedures at
440 the EPMA laboratory of the Max Planck Institute for Chemistry. VM and DK were supported by
441 Russian Foundation for Basic Research (grant No. 16-05-01052). VM was supported by state
442 assignment project No. 0330-2016-0006 and by Russian Science Foundation (grant No. 16-17-10067).

443

444

REFERENCES

445 Agashev, A.M., Pokhilenko, N.P., Tolstov, A.V., Polyanichko, V.V., Malkovets, V.G., Sobolev, N.V.,
446 2004. New age data on kimberlites from the Yakutian diamondiferous province. Doklady Akademii
447 Nauk SSSR, Earth Science Section 399, 1142–1145.

- 448 Agashev, A.M., Ionov, D.A., Pokhilenko, N.P., Golovin, A.V., Cherepanova, Y., and Sharygin, I.S.
449 (2013) Metasomatism in lithospheric mantle roots: Constraints from whole-rock and mineral
450 chemical composition of deformed peridotite xenoliths from kimberlite pipe Udachnaya. *Lithos*,
451 160-161, 201-215.
- 452 Ashchepkov, I.V., Pokhilenko, N.P., Vladykin, N.V., Logvinova, A.M., Afanasiev, V.P., Pokhilenko,
453 L.N., Kuligin, S.S., Malygina, E.V., Alymova, N.A., Kostrovitsky, S.I., Rotman, A.Y., Mityukhin,
454 S.I., Karpenko, M.A., Stegnitsky, Y.B., and Khemelnikova, O.S. (2010) Structure and evolution of
455 the lithospheric mantle beneath Siberian craton, thermobarometric study. *Tectonophysics*, 485, 17-
456 41.
- 457 Ashchepkov, I.V., Pokhilenko, N.P., Vladykin, N.V., Rotman, A.Y., and Afanasiev, V.P. (2008)
458 Reconstruction of mantle sections beneath Yakutian kimberlite pipes using monomineral
459 thermobarometry. *Geological Society Special Publications*, 293, 335-352.
- 460 Boyd, F.R. (1973) A pyroxene geotherm. *Geochimica et Cosmochimica Acta*, 37, 2533-2546.
- 461 Boyd, F.R. (1984) A Siberian geotherm based on lherzolite xenoliths from the Udachnaya kimberlite,
462 U.S.S.R. *Geology*, 12, 528-530.
- 463 Boyd, F.R., Pokhilenko, N.P., Pearson, D.G., Mertzman, S.A., Sobolev, N.V., and Finger, L.W. (1997)
464 Composition of the Siberian cratonic mantle: evidence from Udachnaya peridotite xenoliths.
465 *Contributions to Mineralogy and Petrology*, 128, 228-246.
- 466 Canil, D. (1999) The Ni-in-garnet geothermometer: calibration at natural abundances. *Contributions to*
467 *Mineralogy and Petrology*, 136, 240-246.
- 468 Carswell, D.A. (1991) The garnet–orthopyroxene Al barometer: problematic application to natural
469 garnet lherzolite assemblages. *Mineralogical Magazine*, 55, 19-31.
- 470 Chen, M.M, Tian, W., Suzuki, K., Tejada, M.L.G., Liu, F.L., Senda, R., Wei, C.J., Chen, B., and Chu,
471 Z.Y. (2014) Peridotite and pyroxenite xenoliths from Tarim, NW China: Evidences for melt

- 472 depletion and mantle refertilization in the mantle source region of the Tarim flood basalt. *Lithos*,
473 204, 97-111.
- 474 Cookenboo, H.O., and Grütter, H.S. (2010) Mantle-derived indicator mineral compositions as applied
475 to diamond exploration. *Geochemistry: Exploration, Environment, Analysis*, 10, 81-95.
- 476 Davis, G.L., Sobolev, N.V., and Khar'kiv, A.D. (1980) New data on the age of Yakutian kimberlites
477 obtained by the uranium–lead method on zircons (in Russian). *Doklady AN SSSR*, 254, 175-180.
- 478 Day, H.W. (2012) A revised diamond-graphite transition curve. *American Mineralogist*, 97, 52-62.
- 479 Donnelly, C.L., Stachel, T., Creighton, S., Muehlenbachs, K., and Whiteford, S. (2007) Diamonds and
480 their mineral inclusions from the A154 South pipe, Diavik Diamond Mine, Northwest territories,
481 Canada. *Lithos*, 98, 160-176.
- 482 Doucet, L.S., Ionov, D.A., and Golovin, A.V. (2013) The origin of coarse garnet peridotites in cratonic
483 lithosphere: new data on xenoliths from the Udachnaya kimberlite, central Siberia. *Contributions to*
484 *Mineralogy and Petrology*, 165, 1225-1242.
- 485 Duchkov, A.D., and Sokolova, L.S. (1997) Thermal pattern of the lithosphere of the Siberian Platform
486 (in Russian). *Geologiya i Geofizika*, 38, 494-503.
- 487 Eaton, D.W., Darbyshire, F., Evans, R.L., Grütter, H., Jones, A.G., and Yuan, X. (2009) The elusive
488 lithosphere–asthenosphere boundary (LAB) beneath cratons. *Lithos*, 109, 1-22.
- 489 Faryad, S.W., Dolejš, D., and Machek, M. (2009) Garnet exsolution in pyroxene from clinopyroxenites
490 in the Moldanubian zone: constraining the early pre-convergence history of ultramafic rocks in the
491 Variscan orogen. *Journal of Metamorphic Geology*, 27, 655-671.
- 492 Goncharov, A.G., Ionov, D.A., and Doucet, L.S. (2012) Thermal state, oxygen fugacity and C-O-H
493 fluid speciation in cratonic lithospheric mantle: new data on peridotite xenoliths from the
494 Udachnaya kimberlite, Siberia. *Earth and Planetary Science Letters*, 357-358, 99-110.

- 495 Griffin, W.L., Fisher, N.I., Friedman, J.H., O'Reilly, S.Y., and Ryan, C.G. (2002) Cr-pyrope garnets in
496 the lithospheric mantle. II. Compositional populations and their distribution in time and space.
497 *Geochemistry, Geophysics, Geosystems*, 3, 1073, doi:10.1029/2002GC000298.
- 498 Griffin, W.L., Kaminsky, F.V., Ryan, C.G., O'Reilly, S.Y., Win, T.T., and Ilupin, I.P. (1996) Thermal
499 state and composition of the lithospheric mantle beneath the Daldyn kimberlite field, Yakutia.
500 *Tectonophysics*, 262, 19-33.
- 501 Griffin, W.L., O'Reilly, S.Y., Doyle, B.J., Pearson, N.J., Coopersmith, H., Kivi, K., Malkovets, V., and
502 Pokhilenko, N. (2004) Lithosphere mapping beneath the North American plate. *Lithos*, 77, 873-922.
- 503 Griffin, W.L., Ryan, C.G., Kaminsky, F.V., O'Reilly, S.Y., Natapov, L.M., Win, T.T., Kinny, P.D.,
504 and Ilupin, I.P. (1999) The Siberian lithosphere traverse. Mantle terranes and the assembly of the
505 Siberian craton. *Tectonophysics*, 310, 1-35.
- 506 Grütter, H., Latti, D., and Menzies, A.H. (2006) Cr-saturation arrays in concentrate garnet
507 compositions from kimberlite and their use in mantle barometry. *Journal of Petrology*, 47, 801-820.
- 508 Grütter, H., and Moore, R. (2003) Pyroxene geotherms revisited - an empirical approach based on
509 Canadian xenoliths. Extended Abstract 8th International Kimberlite Conference no. 272.
- 510 Grütter, H.S. (2009) Pyroxene xenocryst geotherms: techniques and application. *Lithos*, 112, 1167-
511 1178.
- 512 Grütter, H.S., and Tuer, J. (2009) Constraints on deep mantle tenor of Sarfartoq-area kimberlites
513 (Greenland), based on modern thermobarometry of mantle-derived xenocrysts. *Lithos*, 112, 124-
514 129.
- 515 Hasterok, D., and Chapman, D.S. (2011) Heat production and geotherms for the continental
516 lithosphere. *Earth and Planetary Science Letters*, 307, 59-70.
- 517 Ionov, D.A., Doucet, L.S., and Ashchepkov, I.V. (2010) Composition of the lithospheric mantle in the
518 Siberian craton: new constraints from fresh peridotites in the Udachnaya-East kimberlite. *Journal of*
519 *Petrology*, 51, 2177-2210.

- 520 Janney, P.E., Shirey, S.B., Carlson, R.W., Pearson, D.G., Bell, D.R., Le Roex, A.P., Ishikawa, A.,
521 Nixon, P.H., and Boyd, F.R. (2010) Age, composition and thermal characteristics of South African
522 off-craton mantle lithosphere: Evidence for a multi-stage history. *Journal of Petrology*, 51, 1849-
523 1890.
- 524 Kopylova, M.G., Russell, J.K., and Cookenboo, H. (1998) Upper-mantle stratigraphy of the Slave
525 craton, Canada: Insights into a new kimberlite province. *Geology*, 26, 315-318.
- 526 Lazarov, M., Woodland, A.B., and Brey, G.P. (2009) Thermal state and redox conditions of the
527 Kaapvaal mantle: A study of xenoliths from the Finsch mine, South Africa. *Lithos*, 112S, 913-923.
- 528 Lehtonen, M., O'Brien, H., Peltonen, P., Kukkonen, I., Ustinov, V., and Verzhak, V. (2009) Mantle
529 xenocrysts from the Arkhangelskaya kimberlite (Lomonosov mine, NW Russia): Constraints on the
530 composition and thermal state of the diamondiferous lithospheric mantle. *Lithos*, 112, 924-933.
- 531 Lepekhina, E.N., Rotman, A.Y., Antonov, A.V., and Sergeev, S.A. (2008a) SHRIMP U-Pb zircon of
532 Yakutian kimberlites pipes. Extended Abstract 9th International Kimberlite Conference, no. 9IKC-
533 A-00354.
- 534 Lepekhina, E.N., Rotman, A.Y., Antonov, A.V., and Sergeev, S.A. (2008b) SHRIMP U-Pb perovskite
535 from kimberlites of the Siberian platform (Verhnemunskoe and Alakite-Marhinskoe fields).
536 Extended Abstract 9th International Kimberlite Conference, no. 9IKC-A-00353.
- 537 Levchenkov., O.A., Gaidamako, I.M., Levskii, L.K., Komarov, A.N., Yakovleva, S.Z., Rizvanova
538 N.G., and Makeev, A.F. (2005) U-Pb age of zircon from the Mir and 325 Let Yakutii Pipes.
539 *Doklady Earth Science*, 400, 99-101.
- 540 Malkovets, V.G., Griffin, W.L., O'Reilly, S.Y., and Wood, B.J., 2007. Diamond, subcalcic garnet, and
541 mantle metasomatism: kimberlite sampling patterns define the link. *Geology* 35 (4), 339–342.
- 542 Manakov, A. (2002) Moho depth beneath the Siberian kimberlite fields. Mirny, Russia. 352 p. PhD
543 thesis.

- 544 Mather, K.A., Pearson, D.G., McKenzie, D., Kjarsgaard, B.A., and Priestley, K. (2011) Constraints on
545 the depth and thermal history of cratonic lithosphere from peridotite xenoliths, xenocrysts and
546 seismology. *Lithos*, 125, 729-742.
- 547 McKenzie, D., and Bickle, M.J. (1988) The volume and composition of melt generated by extension of
548 the lithosphere. *Journal of Petrology*, 29, 625-679.
- 549 McKenzie, D., Jackson, J., and Priestley, K. (2005) Thermal structure of oceanic and continental
550 lithosphere. *Earth and Planetary Science Letters*, 233, 337-349.
- 551 Menzies, A., Westerlund, K., Grütter, H., Gurney, J., Carlson, J., Fung, A., and Nowicki, T. (2004)
552 Peridotitic mantle xenoliths from kimberlites on the Ekati Diamond Mine property, N.W.T., Canada:
553 major element compositions and implications for the lithosphere beneath the central Slave craton.
554 *Lithos*, 77, 395-412. *Chemical Geology*, 368, 97-103.
- 555 Nickel, K.G., and Green, D.H. (1985) Empirical geothermobarometry for garnet peridotites and
556 implications for the nature of the lithosphere, kimberlites and diamonds. *Earth and Planetary
557 Science Letters*, 73, 158-170.
- 558 Nielsen, C.H., and Sigurdsson, H. (1981) Quantitative methods for electron microprobe analysis of
559 sodium in natural and synthetic glasses. *American Mineralogist*, 66, 547-552.
- 560 Nimis, P. (1998) Evaluation of diamond potential from the composition of peridotitic chromian
561 diopside. *European Journal of Mineralogy*, 10, 505-519.
- 562 Nimis, P. (2002) The pressures and temperatures of formation of diamond based on thermobarometry
563 of chromian diopside inclusions. *Canadian Mineralogist*, 40, 871-884.
- 564 Nimis, P., and Grütter, H. (2010) Internally consistent geothermometers for garnet peridotites and
565 pyroxenites. *Contributions to Mineralogy and Petrology*, 159, 411-427.
- 566 Nimis, P., and Taylor, W.R. (2000) Single-clinopyroxene thermobarometry for garnet peridotites. Part
567 I. Calibration and testing of a Cr-in-Cpx barometer and an enstatite-in-Cpx thermometer.
568 *Contributions to Mineralogy and Petrology*, 139, 541-554.

- 569 Nimis, P., Zanetti, A., Dencker, I., and Sobolev, N.V. (2009) Major and trace element composition of
570 chromian diopsides from the Zagadochnaya kimberlite (Yakutia, Russia): Metasomatic processes,
571 thermobarometry and diamond potential. *Lithos*, 112, 397-412.
- 572 O'Reilly, S.Y., and Griffin, W.L. (1985) A xenolith-derived geotherm for southeastern Australia and its
573 geological implications. *Tectonophysics*, 111, 41-63.
- 574 Osako, M., Ito, E., and Yoneda, A. (2004) Simultaneous measurements of thermal conductivity and
575 thermal diffusivity for garnet and olivine under high pressure. *Physics of the Earth and Planetary
576 Interiors*, 143, 311-320.
- 577 Pokhilenko, N.P., Sobolev, N.V., Boyd, F.R., Pearson, D.G., and Shimizu, N. (1993) Megacrystalline
578 pyrope peridotites in the lithosphere of the Siberian platform: Mineralogy, geochemical peculiarities
579 and the problem of their origin. *Russian Geology and Geophysics*, 34, 56-67.
- 580 Pokhilenko, N.P., Sobolev, N.V., Kuligin, S.S., and Shimizu, N. (1999) Peculiarities of distribution of
581 pyroxenite paragenesis garnets in Yakutian kimberlites and some aspects of the evolution of the
582 Siberian craton lithospheric mantle. In: J.J. Gurney, J.L. Gurney, M.D. Pascoe, S.H. Richardson
583 (Eds.), *Proceedings of the 7th International Kimberlite Conference*, vol.2. p. 689-698.
- 584 Pollack, H.N., and Chapman, D.S. (1977) On the regional variations of heat flow, geotherms and
585 lithospheric thickness. *Tectonophysics*, 38, 279-296.
- 586 Potts, P.J., Tindle A.G., and Isaacs, M.C. (1983) On the precision of electron microprobe data: a new
587 test for the homogeneity of mineral standards. *American Mineralogist*, 68, 1237-1242.
- 588 Putirka, K.D. (2008) Thermometers and barometers for volcanic systems. *Reviews in Mineralogy and
589 Geochemistry*, 69, 61-120.
- 590 Ramsay, R.R., and Tompkins, L.A. (1994) The geology, heavy mineral concentrate mineralogy, and
591 diamond prospectivity of the Boa Esperança and Cana Verde pipes, Corrego D'anta, Minas Gerais,
592 Brazil. In: H.O.A. Meyer, O.H. Leonardos (Eds.), *Kimberlites, Related Rocks and Mantle Xenoliths
593 CPRM, Special Publications*, p. 329-345, Brasilia, Brazil.

- 594 Read, G.H., and Janse, A.J.A. (2009) Diamonds: Exploration, mines and marketing. *Lithos*, 112, 1-9.
- 595 Read, G.H., Grütter, H., Winter, S., Luckman, N., Gaunt, F., and Thomsen, F. (2004) Stratigraphic
596 relations, kimberlite emplacement and lithospheric thermal evolution, Quirico' Basin, Minas Gerais
597 State, Brazil. *Lithos*, 77, 803–818.
- 598 Rosen, O.M., Soloviev, A.V., and Zhuravlev, D.Z. (2009) Thermal evolution of the northeastern
599 Siberian Platform in the light of apatite fission-track dating of the Deep Drill Core. *Izvestiya,*
600 *Physics of the Solid Earth*, 45, 914-931.
- 601 Ryan, C.G., Griffin, W.L., and Pearson, N.J. (1996) Garnet geotherms: pressure–temperature data from
602 Cr-pyrope garnet xenocrysts in volcanic rocks. *Journal of Geophysical Research*, 101, 5611-5625.
- 603 Shimizu, N., Pokhilenko, N.P., Boyd, F.R., and Pearson, D.G. (1997) Geochemical characteristics of
604 mantle xenoliths from the Udachnaya kimberlite pipe. *Proceedings of the 6th International*
605 *Kimberlite Conference vol.1, p. 205-217.*
- 606 Shirey, S.B., Cartigny, P., Frost, D.J., Keshav, S., Nestola, F., Nimis, P., Pearson, D.G., Sobolev, N.V.,
607 and Walter, M.J. (2013) Diamonds and the geology of mantle carbon. *Reviews in Mineralogy and*
608 *Geochemistry*, 75, 355-421.
- 609 Smith, D. (1999) Temperatures and pressures of mineral equilibration in peridotite xenoliths: review,
610 discussion, and implications. In: Y. Fei, C.M. Bertka, B.O. Mysen (Eds.), *Mantle petrology: field*
611 *observations and high pressure experimentation: a tribute to Francis R. (Joe) Boyd, vol 6.*
612 *Geochemical Society Special Publications, p. 171-188.*
- 613 Stachel, T., and Harris, J.W. (2008) The origin of cratonic diamonds – constraints from mineral
614 inclusions. *Ore Geology Review*, 34, 5-32.
- 615 Sun, J., Liu, C.Z., Tappe, S., Kostrovitsky, S.I., Wu, F.Y., Yakovlev, D., Yang, Y.-H., and Yang, J.H.
616 (2014) Repeated kimberlite magmatism beneath Yakutia and its relationship to Siberian flood
617 volcanism: insights from in situ U–Pb and Sr–Nd perovskite isotope analysis. *Earth Planet. Sci. Lett.*
618 404, 283-295.

- 619 Taylor, W.R. (1998) An experimental test of some geothermometer and geobarometer formulations for
620 upper mantle peridotites with application to the thermobarometry of fertile lherzolite and garnet
621 websterite. *Neues Jahrbuch für Mineralogie, Abhandlungen*, 172, 381-408.
- 622 Wang, W., and Gasparik, T. (2001) Metasomatic clinopyroxene inclusions in diamonds from the
623 Liaoning province, China. *Geochimica et Cosmochimica Acta*, 65, 611-62.
- 624 Zozulya, D.R., O'Brien, H., Peltonen, P., and Lehtonen, M. (2009) Thermobarometry of mantle-derived
625 garnets and pyroxenes of Kola region (NW Russia): Lithosphere composition, thermal regime and
626 diamond prospectivity. *Bulletin of the Geological Society of Finland*, 81, 143-15.
- 627
- 628
- 629

630 **APPENDIX. PROPAGATION OF ANALYTICAL ERRORS IN SINGLE-CLINOPYROXENE GEOBAROMETRY**

631 The Cr-in-Cpx barometer (Nimis and Taylor, 2000) is expressed as

632
$$P(\text{kbar}) = -\frac{T(\text{K})}{126.9} \cdot \ln a_{\text{Cr}} + 15.483 \cdot \ln \left(\frac{\text{Cr}\#}{T(\text{K})} \right) + \frac{T(\text{K})}{71.38} + 107.8 \quad (1)$$

633 where $a_{\text{Cr}} = \text{Cr} - 0.81 \cdot \text{Na} \cdot \text{Cr}\#$ and $\text{Cr}\# = \text{Cr}/(\text{Cr} + \text{Al})$, with elements in apfu. Although the effect of K
634 on Cpx barometry was unknown, Nimis and Taylor (2000) suggested that any K should be added to Na
635 in P calculations. Assuming random error sources, the uncertainties on pressure estimates can be
636 expressed with a normal error propagation function, i.e.,

637
$$\sigma P = \sqrt{\left(\frac{\partial P}{\partial \text{Cr}} \cdot \sigma_{\text{Cr}} \right)^2 + \left(\frac{\partial P}{\partial \text{Al}} \cdot \sigma_{\text{Al}} \right)^2 + \left(\frac{\partial P}{\partial \text{Na}} \cdot \sigma_{\text{Na}} \right)^2 + \left(\frac{\partial P}{\partial T} \cdot \sigma T \right)^2} \quad (2)$$

638 Calculation of σP requires knowledge of analytical uncertainties on Cr, Al, Na and T . The influence
639 of analytical uncertainties on the very minor K contents can safely be neglected. Uncertainties on T
640 estimates can be derived from reproducibility of temperatures of experiments in two-pyroxene-bearing
641 assemblages using the enstatite-in-Cpx thermometer (± 30 – 40°C ; Nimis and Taylor 2000). Accurate
642 evaluation of EMP uncertainties is not straightforward, because analytical errors primarily depend on
643 both the absolute element concentrations and on the analytical conditions adopted for the analysis.

644 In this appendix, we will investigate the effect of EMP uncertainties on pressure estimates for
645 compositionally diverse clinopyroxenes. As a first step, we will evaluate the analytical errors for
646 different analytical conditions and for a specific set of clinopyroxene compositions through repeat EMP
647 measurements on compositionally homogeneous areas of selected cpx grains, and evaluate the
648 propagated uncertainties on P estimates by calculating P for each analysis. We then apply the error
649 propagation function (Equation 2) to a great variety of natural clinopyroxene compositions, assuming
650 model analytical uncertainties derived from the first test.

651

652 **First step: evaluation of uncertainties vs. analytical conditions**

653 We selected seven clinopyroxenes having a_{Cr} between 0.0016 and 0.0188 apfu, characterized by
654 various proportions of Al, Cr and Na, and equilibrated in a wide range of P – T conditions (Table A1).
655 Appropriate compositions were found in four clinopyroxene xenocrysts from the Novinka kimberlite
656 (this study) and three clinopyroxenes from three well-studied garnet peridotites. Description of the
657 garnet peridotite samples is reported in Supplementary Material S3.

658 Chemical analyses were carried out with a CAMECA SX-50 electron microprobe (IGG–CNR,
659 Padua, Italy), equipped with four wavelength-dispersive spectrometers using one LIF, one PET, and
660 two TAP crystals. Natural and synthetic minerals (diopside for Ca and Si, albite for Na, orthoclase for
661 K, and pure Al, Mg, Cr, Fe, and Mn-Ti oxides) were used as standards. X-ray counts were converted
662 into weight percent oxides by using the CAMECA-PAP program. Each clinopyroxene grain/portion
663 was first analyzed for all elements adopting routine analytical condition, i.e., 1 μ m electron beam, 20
664 kV accelerating voltage, 15 nA beam current, and a counting time of 10 s for peak and 10 s for
665 background (i.e., 5 s on each side of the peak). The most mobile elements were always analyzed first in
666 order to minimize their migration under the electron beam. The sequence of element analyses on each
667 spectrometer was thus as follows: Fe, Mn, Cr (LIF); Si, Al (TAP); Na, Mg (TAP); K, Ca, Ti (PET).
668 This preliminary investigation allowed us to select compositionally homogeneous areas and provided
669 us with average compositions to be used for calculation of matrix effects in subsequent analytical
670 sessions and for preliminary thermobarometry (Table A1).

671 The same clinopyroxenes were then analyzed again for Al, Cr and Na using increasing beam
672 currents and counting times (Table A2). Five analytical sessions were carried out, during which 15
673 individual point analyses were acquired on the same, homogeneous areas of each clinopyroxene. The
674 analyses were carried out on a grid of 3 x 5 analytical spots (maximum side 20 μ m). To limit element
675 migration under the electron beam, before each session the grid was translated by 3–4 μ m, within the
676 previously defined homogeneous areas. Calcium was also measured on the same spots as a further
677 check for compositional homogeneity. The four elements were analyzed simultaneously with the four

678 independent spectrometers. Observed absolute variations in CaO weight percentages between
679 individual point analyses were always ≤ 0.5 wt%. No systematic variations in X-ray counts for Na were
680 observed using different beam currents (i.e., 15 nA and 40 nA), not even after a 300-s count period,
681 implying that Na did not significantly mobilize under the electron beam during our analyses (cf.
682 Nielsen and Sigurdsson 1981). No analyses for which any measured concentration departed by more
683 than 3 standard deviations from the mean were obtained. The average compositions obtained during the
684 five test sessions on each selected clinopyroxene are reported in Table A3.

685 For each point analysis, $Cr\#$, a_{Cr} and Cr-in-Cpx pressure were calculated. Pressures were calculated
686 using fixed input temperature values, which were obtained by applying the enstatite-in-Cpx
687 thermometer, at P given by the Cr-in-Cpx barometer, on the compositions derived from the preliminary
688 analyses of the samples (Table A1). Statistical parameters (mean values, standard deviations, and
689 quantiles) for all relevant variables are reported in Table A3 and illustrated in Figure A1.

690 The relative uncertainties on the measured Al, Cr and Na concentrations decrease smoothly with
691 increasing beam current, counting times, and element abundances (Table A3). This allowed us to
692 model analytical uncertainties as functions of clinopyroxene composition for each set of analytical
693 conditions (Table A4). The standard deviations on P estimates drastically change with changing
694 analytical conditions (σ as high as 1.1 GPa using the lowest beam current and counting times) and
695 clinopyroxene composition (Table A3 and Fig. A1).

696 The relationships between P uncertainties and composition can be explained considering the
697 topology of the Cr-in-Cpx barometer expression (Equation 1). In equation (1), P is related to a_{Cr} and
698 $Cr\#$ through two logarithmic functions. This enhances error propagation with decreasing a_{Cr} and $Cr\#$.
699 Owing to its greater weight in the equation, the effect of the a_{Cr} logarithmic term tends to be dominant
700 in terms of error propagation. This accounts well for the larger P uncertainties obtained for the
701 clinopyroxene Nov-42 ($a_{Cr} = 0.0016$ apfu) with respect to clinopyroxene Uv61/91 ($a_{Cr} = 0.0081$ apfu),
702 in spite of their similar a_{Cr} uncertainties (Table A3). It also explains the progressively larger, non-

703 systematic deviations from orthopyroxene–garnet pressures at lower a_{Cr} (Figs. 2 and 4). Moreover,
704 because of the logarithmic relation, the distribution of propagated errors due to a_{Cr} uncertainties tends
705 to be skewed towards the positive side.

706 Whereas the effect of the $Cr\#$ logarithmic term on error propagation is marginal, $Cr\#$ has a major
707 effect on the uncertainties of the a_{Cr} parameter. In particular, a higher $Cr\#$ will enhance propagation of
708 Na uncertainties on a_{Cr} and, therefore, on P . This explains the lower P uncertainties (and their less
709 pronounced variations between different analytical sessions) obtained for clinopyroxene Nov-80, which
710 is characterized by low a_{Cr} (0.003 apfu) and low $Cr\#$ (0.13), compared with those obtained for
711 compositions with higher $Cr\#$ values (Table A3 and Fig. A1).

712

713 **Second step: P uncertainties in the natural clinopyroxene compositional space and optimum**
714 **analytical conditions for clinopyroxene barometry**

715 The above test showed that the effect of analytical errors on the precision and accuracy of the
716 calculated pressure strongly increases with decreasing a_{Cr} and with increasing $Cr\#$. For any
717 clinopyroxene composition, minimum analytical conditions should be defined for which analytical
718 errors propagate acceptable errors on pressure estimates. For this purpose, a more extended test on a
719 comprehensive set of clinopyroxene compositions is needed. We have used the database of well-
720 equilibrated xenoliths of Nimis and Grütter (2010) as our test material. Temperatures for each xenolith
721 were calculated using the thermometer of Taylor (1998) at P given by the orthopyroxene–garnet
722 barometer of Nickel and Green (1985; with modifications by Carswell 1991, his equations E6 and E9,
723 assuming no ferric iron). The T uncertainty was fixed at 40 °C (cf. Nimis and Taylor 2000).
724 Uncertainties on clinopyroxene Cr, Al and Na analyses were calculated for each xenolith for five
725 combinations of analytical conditions, taking into account the results of our previous analytical test
726 (Table A4). Uncertainties on Cr-in-Cpx pressures were then calculated by normal error propagation of
727 the five resulting sets of analytical uncertainties (Equation 2).

728 As expected, the calculated uncertainties increase with decreasing a_{Cr} and increasing $Cr\#$ values
729 (Fig. 3), reaching 1.8 GPa when a_{Cr} is <0.002 apfu and the lowest current and counting times are
730 assumed. These results can be used to determine an approximate compositional threshold below which
731 pressure estimates become too sensitive to analytical errors. We consider a propagated uncertainty of
732 ± 0.25 GPa on the calculated P , including the effect of both analytical and thermometric errors, to be a
733 reasonable limit. Taking into account the standard error of estimate of the barometer calibration (± 0.23
734 GPa), this limit should ensure an overall uncertainty smaller than ± 0.4 GPa. We found that simplified
735 thresholds based on the $a_{Cr}/Cr\#$ ratio (Table A2) permit discrimination of compositions for which P
736 uncertainties are acceptable to within a 95% confidence limit.

737

738

739 **Figure 1.** Sketch tectonic map of the Siberian platform with major kimberlite fields. Terranes are
740 outlined by dashed curves and are named in italic. Modified after Griffin et al. (1999).

741 **Figure 2.** Discrepancies between the Cr-in-Cpx barometer (Nimis and Taylor 2000; P_{NT00}) and the
742 orthopyroxene-garnet barometer (P_{Ca91} ; Nickel and Green 1985, as modified by Carswell 1991) vs. the
743 clinopyroxene parameter a_{Cr} . Clinopyroxene compositions are from the compilation of well-
744 equilibrated garnet peridotite and pyroxenite xenoliths of Nimis and Grütter (2010). In **(a)** the entire
745 dataset has been included, while in **(b)** only clinopyroxene plotting in the high-Al field of Nimis (1998)
746 [$Al_2O_3 \geq 0.7$ wt%; $Al_2O_3 \geq 12.175 - 0.6375 * MgO$ wt%] and having $Cr\#$ between 0.06 and 0.50
747 (Grütter, 2009) have been plotted. The overall shift of high- P clinopyroxenes towards negative values
748 can be ascribed to the known underestimation of PNT00 at high P (cf. Nimis 2002).

749 **Figure 3.** Calculated P uncertainties (σ) vs. a_{Cr} for clinopyroxenes from well-equilibrated garnet
750 peridotites and pyroxenites (database of Nimis and Grütter 2010). The P uncertainties were calculated
751 from normal propagation of T uncertainties ($\pm 40^\circ C$) and analytical errors derived from equations
752 reported in Table A4 assuming **(a)** the lowest beam current (15 nA) and counting times (10 s peak, 5 +
753 5 s background) and **(b)** the highest beam current (40nA) and counting times (40 s peak, 20 + 20 s
754 background).

755 **Figure 4.** P estimates using the Cr-in-Cpx barometer (Nimis and Taylor 2000; P_{NT00}) plotted versus P
756 estimates using the orthopyroxene-garnet barometer of Nickel and Green (1985, as modified by
757 Carswell 1991; P_{Ca91}) for **(a)** the entire dataset of well equilibrated garnet peridotites and pyroxenites of
758 Nimis and Grütter (2010) and **(b)** the same dataset excluding samples with calculated Cr-in-Cpx
759 pressure uncertainties greater than ± 0.25 GPa.

760 **Figure 5.** Results of single-clinopyroxene thermobarometry (Nimis and Taylor 2000) for the Novinka
761 kimberlite. In **(a)** the accepted analyses have been selected on the basis of the revised protocol for
762 single-clinopyroxene thermobarometry (this work), which takes into account the results of our
763 analytical test (Appendix). For comparison, plot **(b)** shows the results of the filtering protocol of

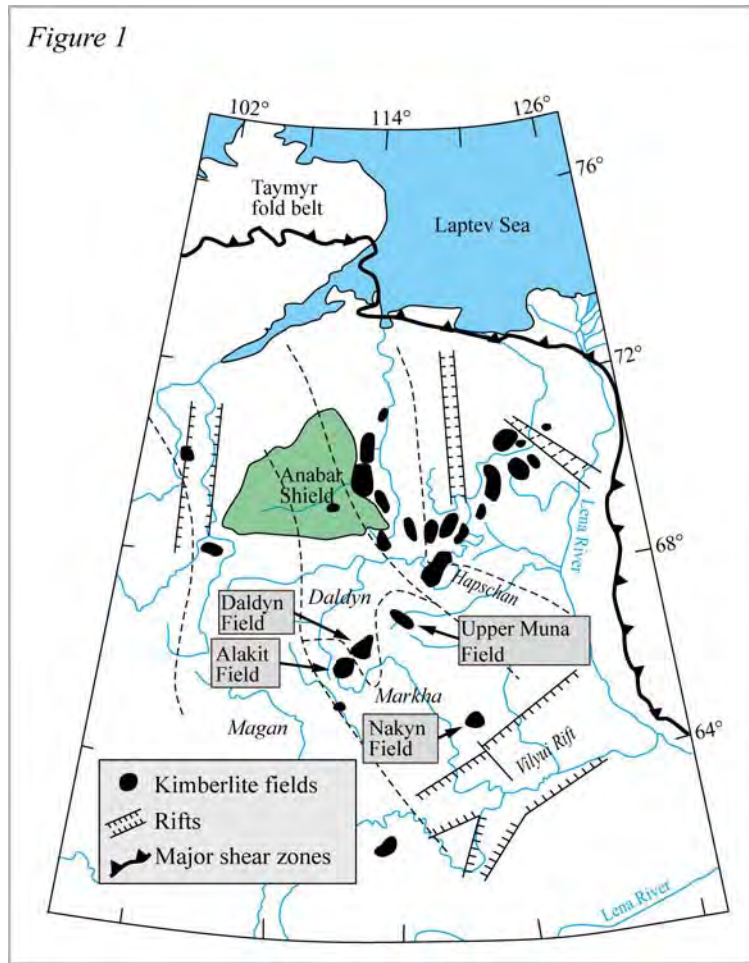
764 Grütter (2009) applied on the same initial dataset (97 routine analyses; see text). Dashed curves are
765 classical reference conductive geotherms for different surface heat-flows (mW/m^2) after Pollack and
766 Chapman (1977). The graphite (G) - diamond (D) boundary (solid curve) is after Day (2012).

767 **Figure 6.** Model palaeogeotherms calculated using the program FITPLOT (McKenzie et al. 2005). The
768 palaeogeotherm for Novinka are calculated **(a)** using all P - T estimates based on optimized
769 clinopyroxene analyses and **(b)** excluding data plotting above 5.5 GPa. The smaller plots show P - T
770 data for Udachnaya xenoliths, calculated using the geothermometer of Nimis and Taylor (2000; T_{NT00})
771 in combination with **(c)** the Nickel and Green (1985; P_{NG85}) geobarometer, **(d)** its modification by
772 Carswell (1991; P_{Ca91}), and **(e)** the Cr-in-Cpx geobarometer of Nimis and Taylor (2000; P_{NT00}). Grey
773 symbols in **(e)** indicate clinopyroxenes for which the calculated σ_P is > 0.25 GPa (taking into account
774 the analytical conditions used for the analysis as reported in the source papers). Source mineral
775 compositions for Udachnaya are from Boyd (1984), Pokhilenko et al. (1993), Shimizu et al. (1997),
776 Ionov et al. (2010), Goncharov et al. (2012), and Doucet et al. (2013).

777 **Figure 7.** Relationships between P/T gradients, $a_{\text{Cr}}/\text{Cr}\#$ in clinopyroxene, and uncertainties of Cr-in-
778 Cpx pressure propagated from analytical errors. Filled circles are $a_{\text{Cr}}/\text{Cr}\#$ values of the experimental
779 clinopyroxenes used for the calibration of the Cr-in-Cpx barometer (Nimis and Taylor 2000), empty
780 squares are $a_{\text{Cr}}/\text{Cr}\#$ values of natural clinopyroxenes from well-equilibrated peridotites (Nimis and
781 Grütter 2010) and crosses are calculated P uncertainties for the same dataset (see Fig. 3 and text for
782 calculation methods). Natural clinopyroxenes with $\text{Cr}\# < 0.1$, which are considered unsuitable for
783 geobarometry (see text), were excluded from the plot. The approximate correspondence between P/T
784 gradients and steady-state continental geotherms (Pollack and Chapman 1977) is also indicated at the
785 top of the plot. Geobarometry of clinopyroxenes from relatively cold mantle sections ($< 40 \text{ mW/m}^2$) is
786 clearly more sensitive to propagation of analytical errors.

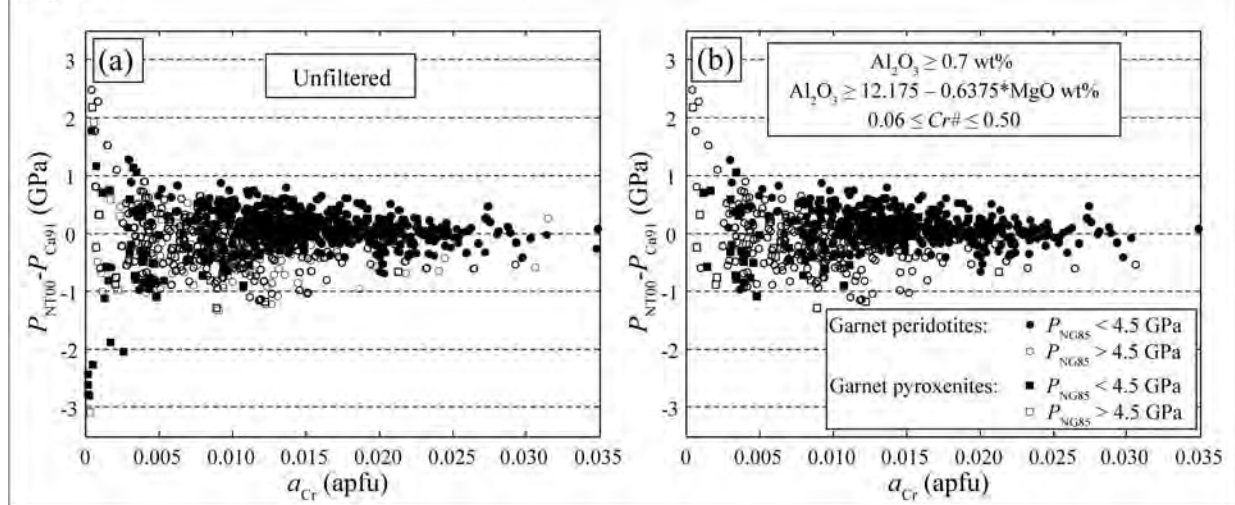
787

Figure 1



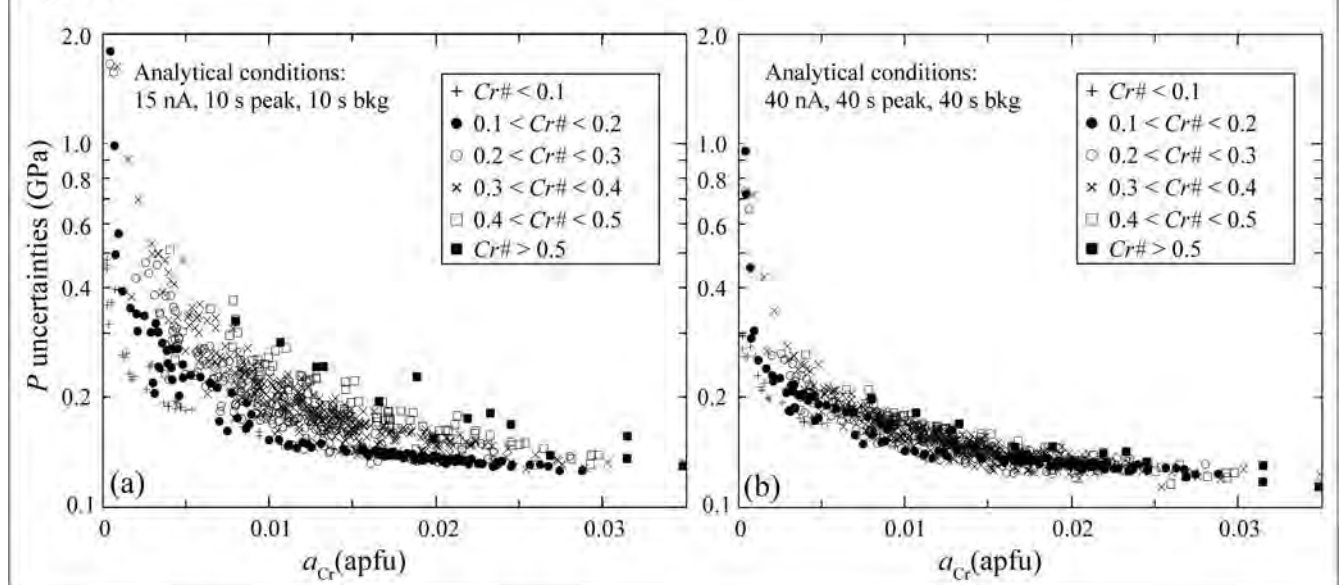
794

Figure 2



795

Figure 3

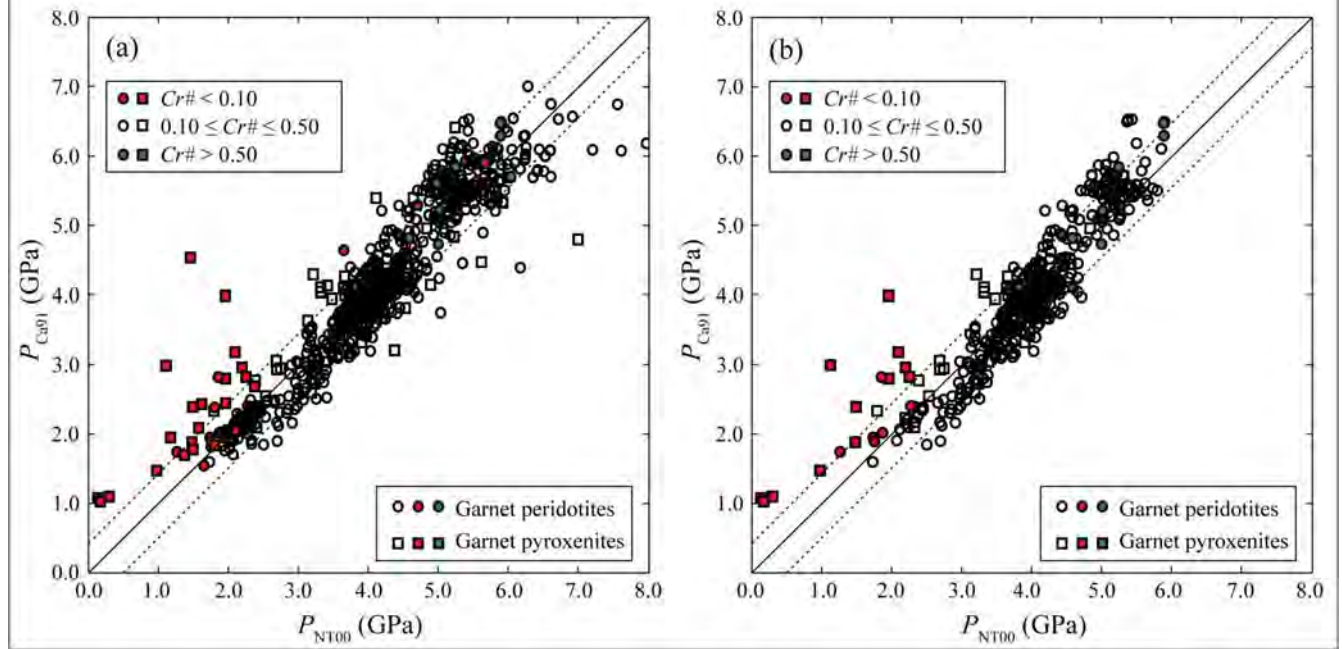


796

797

798

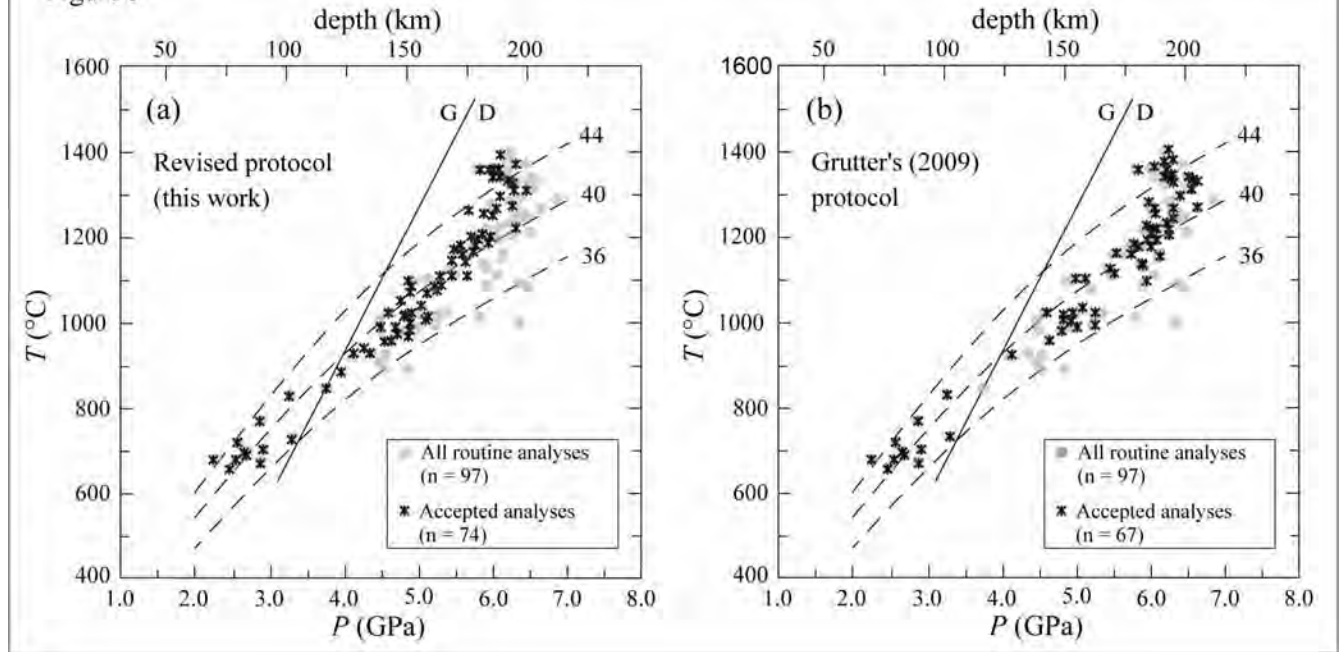
Figure 4



799

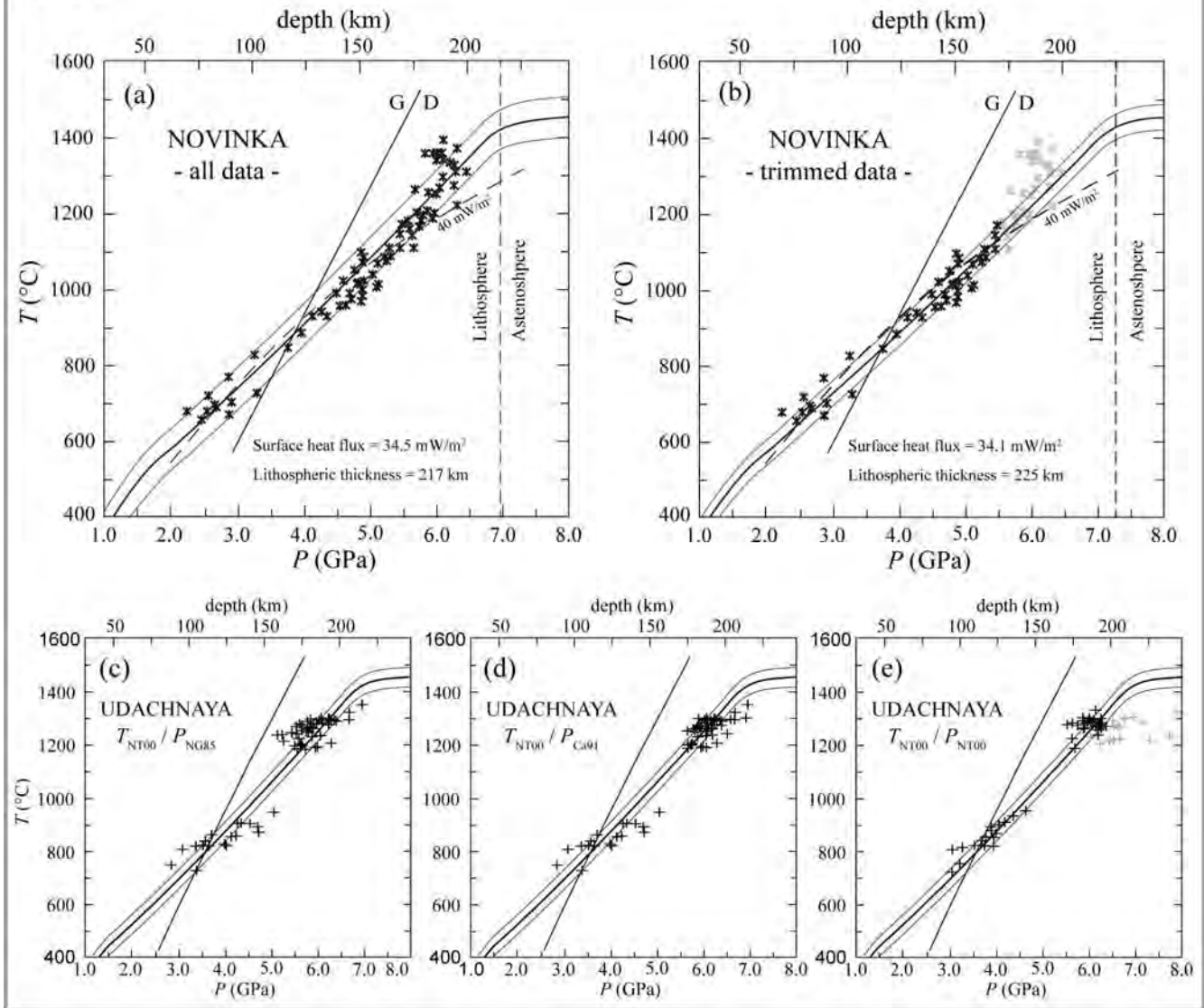
800

Figure 5



801

Figure 6

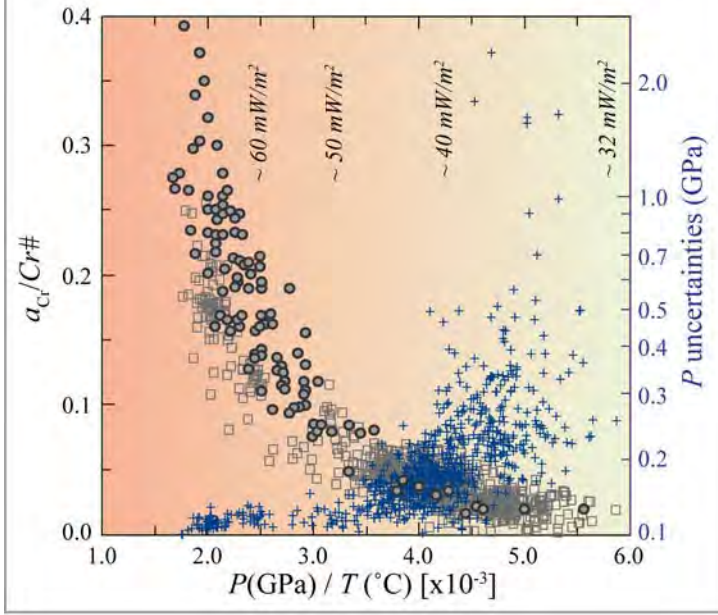


802

803

804

Figure 7



805

806